Available online at www.sciencedirect.com

SciVerse ScienceDirect

Ceramics International 39 (2013) 5227–5234

CERAMICS INTERNATIONAL

www.elsevier.com/locate/ceramint

Preparation and characterization of Co^{2+} substituted Li–Dy ferrite ceramics

U.B. Shinde[a], Sagar E. Shirsath[b,*], S.M. Patange[c], S.P. Jadhav[d], K.M. Jadhav[e], V.L. Patil[f]

[a]S. P. Women's Engineering College, Aurangabad, MS, India
[b]Spin Device Technology Center, Faculty of Engineering, Shinshu University, Nagano 380-8553, Japan
[c]Materials Research Laboratory, Srikrishna Mahavidyalaya Gunjoti, Omerga, Osmanabad 413613, MS, India
[d]Department of Chemistry, Adarsh College, Omerga 413613, MS, India
[e]Department of Physics, Dr. Babasaheb Ambedkar Marathwada University, Aurangabad 431004, MS, India
[f]Vishwakarma Institute of Information Technology, Pune, MS, India

Received 31 October 2012; received in revised form 7 December 2012; accepted 7 December 2012
Available online 20 December 2012

Abstract

Stoichiometric compositions of ferrites with the chemical formula $Li_{0.5-0.5x}Co_xFe_{2.4-0.5x}Dy_{0.1}O_4$ with $x=0$, 0.25, 0.5, 0.75, 1.0 were prepared by the standard double sintering ceramic method. X-ray diffraction analysis confirmed the cubic spinel structure of the prepared samples. The structural, morphological and magnetic properties were studied by X-ray diffraction, infra-red spectroscopy (IR), scanning electron microscopy (SEM), vibrating sample magnetometry (VSM) and ac susceptibility measurements. Lattice constant, grain size and density increase whereas porosity decreases with the increase in Co^{2+} substitution. IR measurements show the characteristic ferrite bands. Spectral absorption bands were observed in IR spectroscopic analysis at $v_1=564-601\ cm^{-1}$, $v_2=486-519\ cm^{-1}$ and $v_3=551-578\ cm^{-1}$. The cation distribution estimated by the X-ray diffraction is supported by magnetization and susceptibility studies. The saturation magnetization decreases from 44.25 to 17.14 emu/g whereas coercivity remarkably increases from 240.69 to 812.14 emu/g with increasing Co^{2+} substitution. The mechanisms involved are discussed.

Keywords: C. Magnetic properties; Li–Dy ferrites; XRD; IR

1. Introduction

Ferrite with the spinel structure is the most widespread material in the radio engineering, automatics, and computer facilities. The crystal structure of these materials controls their magnetic, electrical, and physical properties [1]. The polycrystalline ferrites have very important structural, magnetic and electrical properties that are depend on the several factors such as method of preparation, substitution of cations and microstructure, etc. Lithium ferrite and substituted lithium ferrites have interesting technological applications [2–7]. Lithium ferrite substituted with the magnetic and nonmagnetic cation is a well-known promising candidate for microwave applications [8]. Lithium and substituted lithium ferrites have remained excellent materials in high density recording media and absorbers due to their typical magnetic properties [9–11]. Lithium ferrite is a low-cost substitute to the garnet based materials for the microwave applications and is a promising candidate for cathode materials in rechargeable lithium batteries [12,13]. Crystal structure, microstructure and cation distribution have remarkable effects on the properties of ferrite material and its applied aspects [14]. Substitution of various ions like Cd [15], Zn [16], Mg [17], Cr [18] in the lithium ferrite matrix have been studied by many researchers. The influence of rare earth oxide (R_2O_3) on the structural, magnetic and electrical properties of Li–Zn ferrite was examined by Rezlescu et al. [19]. Their results reveal that by introducing a relatively small amount of R_2O_3 instead of Fe_2O_3, an important modification in structural properties can be obtained. The combination of the three classes of elements

*Corresponding author. Tel.: +81 8048186605; fax: +91 2402361270.
E-mail address: shirsathsagar@hotmail.com (S.E. Shirsath).

0272-8842/$ - see front matter © 2012 Elsevier Ltd and Techna Group S.r.l. All rights reserved.
http://dx.doi.org/10.1016/j.ceramint.2012.12.022

{(Li, Co), (R_2O_3) and (Fe)} in one compound may lead to materials that have high magnetic ordering temperature and large magnetization as well as large magnetocrystalline anisotropy. The presence of small amount of rare earth ions like Yb, Er, Sm, Tb, Gd, Dy, and Ce modified the properties of $Ni_{0.7}Zn_{0.3}Fe_2O_4$ ferrite [20]. Shirsath et al. shows that the small substitutions of Fe ions by Dy^{3+} rare earths ions may favorably influence the magnetic properties of ferrite and therefore, it is thus possible to obtain a good magnetic material for any tailor-made application [21]. Jing et al. [22] studied the role of rare earth ions in W type ferrite and concluded that Dy substituted ferrite composite has excellent microwave absorption properties. Cobalt (Co^{2+}) possesses the high anisotropy constant and has high magnetic moment (3 μ_B). Several kinds of $CoFe_{2-x}RE_xO_4$ nanoparticles (RE=La, Ce, Nd, Sm, Gd, Tb, Ho) synthesized by the so-called polyol method was reported by Tahar et al. [23]. Further they concluded that the spin-orbital coupling is usually much stronger in rare earth ions than in the first row transition metal ions, and would contribute in increasing the blocking temperature and the coercivity when the RE^{3+} ions partially replace Fe^{3+} in $CoFe_2O_4$ nanoparticles, particularly when RE^{3+} are anisotropic. Ahmed et al. studied the physical properties of LiCo-ferrite with constant lithium:cobalt ratio of (6:1) and doped with different amounts of ytterbium in order to improve the dielectric behavior of the investigated ferrite [24]. They also studied the role of the Dy-content on the magnetic properties of LiCo-ferrite and found an anomalous behavior of the samples with a Dy-content of 0.075 [25].

In this work, an attempt has been made to study the structural and magnetic properties of cobalt substituted lithium ferrite in the presence of rare earth (Dy^{3+}) ion in small amount. However, to the best of our knowledge no systematic studies have been found in the literature regarding the structural and magnetic properties of $Li_{0.50-0.5x}Co_xFe_{2.4-0.5x}Dy_{0.1}O_4$.

2. Experimental techniques

Lithium–cobalt mixed ferrites with a chemical formula $Li_{0.50-0.5x}Co_xFe_{2.4-0.5x}Dy_{0.1}O_4$ where $x=0.0$, 0.25, 0.5, 0.75, 1.0 have been prepared by the standard double sintering ceramic method using AR grade (purity 99.9%) Fe_2O_3, CoO, Li_2Co_3, Dy_2O_3. Intimate mixtures of all the samples, after weighing in the correct stoichiometric proportions of the constituent oxides, were ground thoroughly to obtain good homogeneity. The samples were then pre-sintered at 1173 K for 12 h. The pre-sintered powders were again ground and granulated using 5% poly-vinyl alcohol as a binder. The granulated mixture was then palletized at a pressure of 6 ton/in^2, the samples were finally sintered at 1323 K for 12 h in air and slowly cooled to room temperature. Sintering was carried out with a heating rate of ~5 K/min, whereas cooling rate is around 3 K/min.

The samples were X-ray examined by a Phillips X-ray diffractometer (Model 3710) using Cu K_α radiation ($\lambda=1.5405$ Å). The microstructure and morphology of sintered powder were characterized by scanning electron microscopy (SEM) on a JEOL-JSM-5600N scanning electron microscope. The infrared spectra of all the samples were recorded at room temperature in the range of 200–800 cm^{-1} on a Perkin Elemer spectrometer (model 783). To study the IR spectra of all the samples, about 1 mg of fine powder of each sample was mixed with KBr in the ratio 1:250 by weight to ensure uniform distribution in the KBr pellet. The mixed powder was then pressed in a cylindrical die to obtain the circular disc of approximately 1 mm thickness. Magnetic measurements were performed using the commercial PARC EG&G vibrating sample magnetometer VSM 4500. Magnetic hysteresis loops were measured at room temperature with maximum applied magnetic fields up to 0.5 T. The ac susceptibility double coil set up operating at a frequency of 263 Hz and in rms field of 100 Oe was used to record the temperature variation susceptibility. The susceptibility apparatus was calibrated with nickel prior to the measurements.

3. Results and discussion

3.1. Structural aspects

Fig. 1 shows the typical X-ray diffraction pattern of the $Li_{0.25}Fe_{2.15}Co_{0.5}Dy_{0.1}O_4$ (i.e. $x=0.5$). The XRD pattern clearly shows two phases corresponding to cubic spinel structure and secondary phase due to Dy^{3+} ions. The addition of rare earth ions is believed to act as a sintering catalyst helping in the development of the solid solutions at lower temperature. Rare earth doped system may have secondary phases of Fe_2O_3 and $DyFeO_3$ rather than the pure single phase. There are many parameters affecting the role of rare earth behavior. The most important parameters are electronic configuration and the ionic radii. The rare earth ions have large ionic radii and thus cannot occupy the available tetrahedral or octahedral sites, this leads to

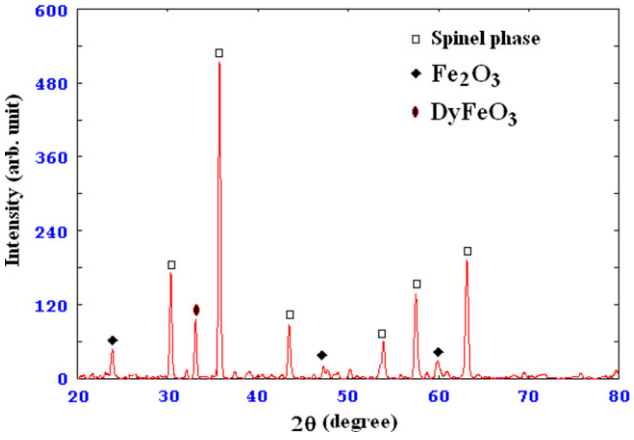

Fig. 1. X-ray diffraction pattern of a typical sample $x=0.5$.

formation of secondary phases [26]. Bharathi et al. have also identified the $DyFeO_3$ phase in $NiOFe_{1.925}Dy_{0.075}O_3$ [27].

The 'd' spacing values were calculated for the recorded peaks using Bragg's law and the lattice constant 'a' was calculated for each plane. The average lattice parameter 'a' can also be obtained by calculating the average of the 'a' values for each sample. The extrapolation function $F(\theta)$ i.e. the Nelson–Riley function for each reflection of the studied sample was calculated [28]

$$F(\theta)=\frac{1}{2}\left[\left(\frac{\mathrm{Cos}^2\theta}{\mathrm{Sin}\,\theta}\right)+\left(\frac{\mathrm{Cos}^2\theta}{\theta}\right)\right] \quad (1)$$

The values of the lattice constant 'a' are drawn as a function of $F(\theta)$ for all the x values (figure not shown here). The true values of the lattice parameter 'a_0' can easily be obtained by extrapolating the line to the value $F(\theta)=0$ or $\theta=90^\circ$. The true values of the lattice constant 'a_0' are listed in Table 1. As indicated in Table 1 that there is a small deviation between the true 'a_0' and average 'a' value of the lattice constant. Generally, the true values of the lattice constant are little smaller than that of average 'a' values. It is clear that both 'a_0' and 'a' increased as the cobalt substitution increased. This can be related to the fact that the cobalt ion has a radius of 0.72 Å, which is larger than that of Fe^{3+} (0.67 Å). When the larger cobalt ions enter in the lattice, the unit cell expands while preserving the overall cubic symmetry.

The experimental density (ρ_{exp}) was determined using the Archimedes' principle [29]. The specimen was weighed in air and in xylene at room temperature, ρ_{exp}=weight of the sample in air/loss of weight in the xylene. The X-ray density ($\rho_{x\text{-}ray}$) was determined using the relation $\rho_{x\text{-}ray}=8M/Na^3$ where, M is the molecular weight of the sample, N is the Avogadro's number and 'a' is lattice constant. The experimental densities (ρ_{exp}) of the specimens were about 95–98% of the corresponding X-ray density ($\rho_{x\text{-}ray}$). The values of $\rho_{x\text{-}ray}$ and porosity are given in Table 1. It is clear from Table 1 that the increase in composition x increase the $\rho_{x\text{-}ray}$. The increase in the density is correlated with an increase of atomic weight of the substituted Co^{2+} ions instead of Fe^{3+} ions of lower atomic mass. The atomic weights of Co^{2+} and Fe^{3+} are 58.94 and 55.845 amu, respectively. The percentage porosity (P) of each sample was calculated by using the relation, porosity$=(\rho_{x\text{-}ray}-\rho_{exp})/\rho_{x\text{-}ray}$. Values of the percentage porosity are given in Table 1. It is observed that porosity increase with increasing amount of Co^{2+}. The increase in porosity may be due to the increase of oxygen vacancies.

Table 1
Average lattice constant (a), true lattice constant (a_0), X-ray density ($\rho_{x\text{-}ray}$) and porosity (P).

x	a (Å)	a_0 (Å)	$\rho_{x\text{-}ray}$ (g/cm^3)	P (%)
0.00	8.328	8.324	5.261	3.07
0.25	8.339	8.333	5.336	3.67
0.50	8.359	8.352	5.392	4.11
0.75	8.371	8.369	5.463	6.27
1.00	8.384	8.378	5.531	7.25

SEM images of typical samples $x=0.25$, 0.50 and 0.75 are shown in Fig. 2. As revealed from these images that all the samples exhibited well densified microstructure. The average grain size was smaller than 2 μm. The smaller grain size will be helpful to increase the resistivity and decrease the eddy current loss at high frequency.

The cation distribution in the present system was obtained from an analysis of the X-ray diffraction patterns. In this method the observed intensity ratios were compared with the calculated intensity ratios. Bertaut method [30] was used to determine the cation distribution. This method selects a few pairs of reflections in accordance to the expression

$$\frac{I_{hkl}^{Obs.}}{I_{h'k'l'}^{Obs.}}=\frac{I_{hkl}^{Calc.}}{I_{h'k'l'}^{Calc.}} \quad (2)$$

where $I_{hkl}^{Obs.}$ and $I_{hkl}^{Calc.}$ are the observed and calculated intensities for the reflection (hkl), respectively. The best information on the cation distribution is achieved by comparing the experimental and calculated intensity ratios for reflections whose intensities (i) are nearly independent of the oxygen parameter, (ii) vary with the cation distribution in opposite ways and (iii) do not significantly differ.

In the present work the reflections of (220), (400), and (440) were used to calculate the intensity ratio. These planes are assumed to be sensitive to the cation distribution [31–33]. Also Fe_2O_3 and $DyFeO_3$ phases are considered. The temperature and absorption factors are not taken into account in our calculations as they do not affect the intensity calculation. If an agreement factor (R) is defined as given in Eq. (3), the best-simulated structure which matches the actual structure of the sample will lead to a minimum value of R and the corresponding cation distribution is obtained for each hkl and $h'k'l'$ reflection pair considered.

$$R=\left|\left(\frac{I_{hkl}^{Obs.}}{I_{h'k'l'}^{Obs.}}\right)-\left(\frac{I_{hkl}^{Calc.}}{I_{h'k'l'}^{Calc.}}\right)\right| \quad (3)$$

The intensities of these are nearly independent of the oxygen parameters. The calculations were made for various combinations of cations. For the calculation of the relative integrated intensity of a given diffraction line from powder specimens as observed in a diffractometer with a flat-plate sample holder, the following formula is valid:

$$I_{hkl}=|F|_{hkl}^2 P L_P \quad (4)$$

where F is structure factor, P is multiplicity factor, L_P the Lorentz polarization factor and

$$L_P=\frac{1+\cos^2 2\theta}{\sin^2\theta\cos\theta} \quad (5)$$

The atomic scattering factor for various ions was taken from the literature [34]. The resultant cation distribution

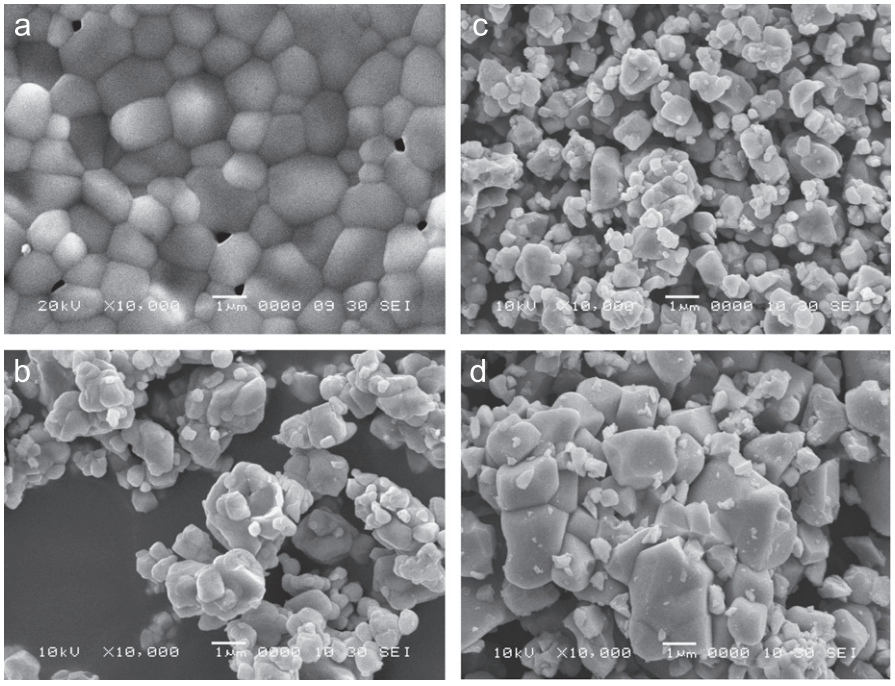

Fig. 2. Scanning electron micrographs of (a) $x=0.0$, (b) $x=0.25$, (c) $x=0.50$ and (d) $x=0.75$.

Table 2
The estimated cation distribution of $Li_{0.5-0.5x}Co_xFe_{2.4-0.5x}Dy_{0.1}O_4$.

x	A-site	B-site
0.00	$Li_{0.096}Dy_{0.002}Fe_{0.902}$	$Li_{0.404}Dy_{0.098}Fe_{1.498}$
0.25	$Li_{0.06}Dy_{0.009}Fe_{0.931}$	$Li_{0.315}Co_{0.25}Dy_{0.091}Fe_{1.344}$
0.50	$Li_{0.023}Dy_{0.012}Fe_{0.965}$	$Li_{0.227}Co_{0.5}Dy_{0.088}Fe_{1.185}$
0.75	$Li_{0.01}Dy_{0.013}Fe_{0.977}$	$Li_{0.115}Co_{0.75}Dy_{0.087}Fe_{1.048}$
1.00	$Dy_{0.018}Fe_{0.982}$	$Co_1Dy_{0.082}Fe_{0.918}$

obtained in this way is presented in Table 2. It is seen from Table 2 that Dy^{3+} ions distributed over both the sites and showing preference toward B-site. Our results are in good agreement with the assumption of Smit and Wijn [35] and Ahmed and Bishay [24].

The mean ionic radius of the tetrahedral (A) and octahedral [B] site (r_A and r_B) can be calculated using the relations discussed elsewhere [36]. The variation in r_A and r_B are presented in Fig. 3. It is clear from Fig. 3 that the r_A decrease whereas r_B increase with increasing Co^{2+} substitution. Discrepancy in the decrease of the tetrahedral or the increase in the octahedral radius may be attributed to the relative value of the occupancy of Li^+, Co^{2+}, Dy^{3+} and Fe^{3+} with their different ionic radii of 0.78 Å, 0.72 Å, 0.99 Å and 0.67 Å respectively in the tetrahedral and octahedral site. The theoretical lattice parameter (a_{th}) can be calculated from the following relation [37]:

$$a_{th}=\left(\frac{8}{3\sqrt{3}}\right)[r_A+R_0]+\sqrt{3}[r_B+R_0] \quad (6)$$

Values of theoretical lattice parameters are shown in Fig. 4. The values of a_{th} lie between 8.229 Å and 8.688 Å

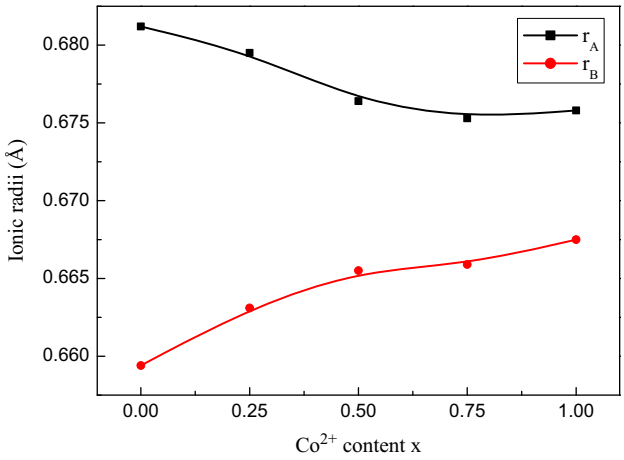

Fig. 3. Variation of mean ionic radii of tetrahedral-A- site (r_A) and octahedral B-site (r_B) with Co^{2+} content x.

which agree with that of 'a' and 'a_0' however the values of 'a_{th}' are little higher than the values of 'a' and 'a_0'.

Using values of 'a', radius of the oxygen ion $R_O=1.32$ Å and 'r_A' in the following expression, the oxygen positional parameter 'u' can be calculated [38]

$$u=\left[(r_A+R_0)\frac{1}{\sqrt{3}a}+\frac{1}{4}\right] \quad (7)$$

Fig. 4 shows the increasing value of oxygen positional parameter 'u' from 0.3888 to 0.3891 Å. In the most oxide spinels the oxygen ions are larger than the metallic ions. In spinel like structure the oxygen positional parameter has a value near 0.375 Å for which the arrangement of O^{2-} ions is exactly a cubic closed packing but in an actual spinel

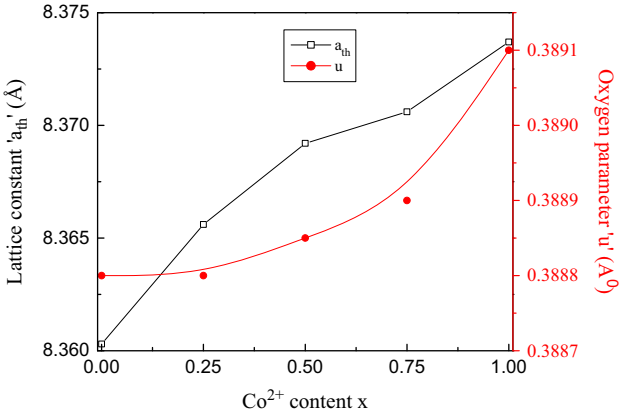

Fig. 4. Theoretical lattice constant (a_{th}) and oxygen positional parameter (u) of $Li_{0.5-0.5x}Co_xFe_{2.4-0.5x}Dy_{0.1}O_4$.

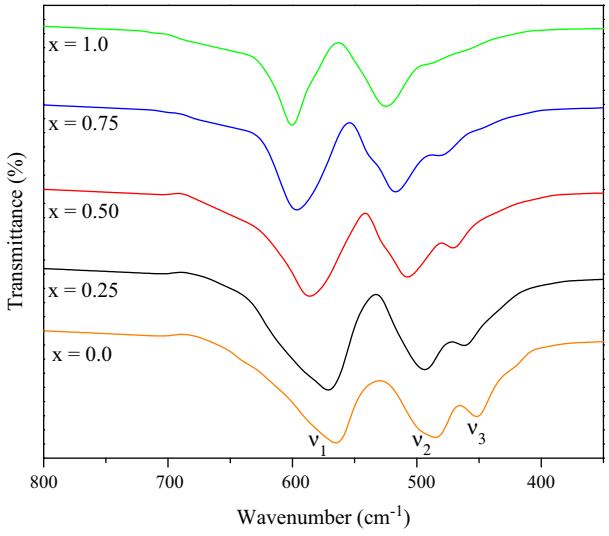

Fig. 5. Infrared spectra of $Li_{0.5-0.5x}Co_xFe_{2.4-0.5x}Dy_{0.1}O_4$.

lattice, this ideal pattern is slightly deformed. The lattice disturbance is confirmed by the data for the lattice constant and the oxygen positional parameter.

3.2. Spectral aspects

Infrared spectroscopy may be used to determine the local symmetry in crystalline solids and it also put light on the ordering phenomenon in the spinel structure [39]. The cubic spinel, with the space group of $Fd3mO_h^7$ has four infrared active vibrations. The substitution of the different ions changes the parameters like the metal oxygen bond strength, the metal oxygen bond length and dimensions of the unit cell. All these parameters affect the infrared spectrum. The IR absorption spectra of the present system were recorded in the wavenumber range of 200–800 cm^{-1} and were shown in Fig. 5. Vibrational band frequency (ν_1, ν_2 and ν_3) obtained from IR spectra are given in Table 3. The first two bands ν_1 and ν_2 appeared at around 600 cm^{-1} and 400 cm^{-1} respectively were attributed to the Fe^{3+}–O

Table 3
Vibration band frequency (ν_1, ν_2 and ν_3) from IR.

x	ν_1 (cm^{-1})	ν_2 (cm^{-1})	ν_3 (cm^{-1})
0.00	564	486	451
0.25	573	493	459
0.50	587	508	471
0.75	597	516	478
1.00	601	519	–

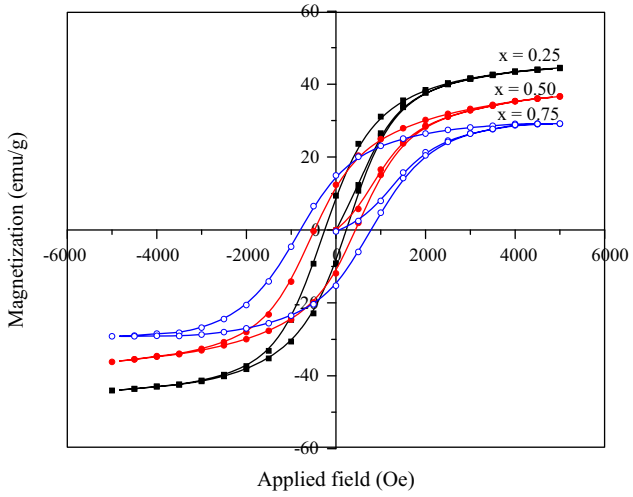

Fig. 6. Plots of magnetization versus applied field.

bonds on the tetrahedral-A and octahedral-B site respectively [40]. Band ν_3 was attributed to Li^+–O bonds of octahedral-B site. Band ν_4 in the basic composition $x=0.0$ was attributed to the lattice vibration. With the addition of cobalt ions the intensity of the Li–O bands decreases and completely disappears for higher cobalt substitution. The shift in the position of ν_2 bands toward the higher frequency side suggests the occupancy of Co^{2+} ions at octahedral B-site. However, due to the substitution of Co^{2+} ions the broadening of ν_2 bonds takes place which may be due to the occupancy of cations of different characters in the same site. The intensity of vibrations at octahedral B-site reveals a distortion of octahedron where large dysprosium ions are occupied. The slight but distinct displacement of absorption band with increasing composition factor x indicates the increasing incorporation of Co^{2+} ion at B-site.

3.3. Magnetic aspects

Fig. 6 shows the curve of magnetization with applied field for the typical samples ($x=0.25$, 0.50 and 0.75). The magnetization curve reveals that the change in the magnetic behavior with Co^{2+} substitution. The magnetization curves are used to get the values of saturation magnetization (M_s), remanent magnetization (M_r) and coercivity (Hc). The variation of saturation magnetization

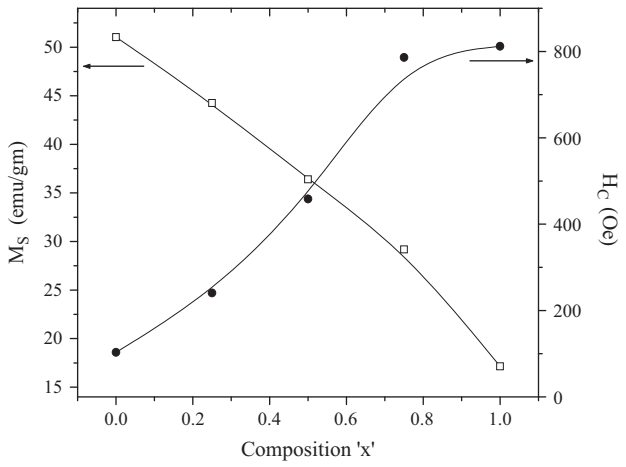

Fig. 7. Variation of saturation magnetization (M_s) and coercivity (H_c) with Co^{2+} content x.

and coercivity is shown in Fig. 7. It is observed from Fig. 7 that the saturation magnetization decreases whereas coercivity increases with Co^{2+} substitution.

According to the Neel's two sublattice collinear spin model, the magnetization depends on the cation distribution in the A- and B-site. The spins at both sites are coupled anti-ferromagnetically leading to the net magnetization per formula unit at 0 K (M_s) which is simply the numerical difference between the sublattice magnetization. Keeping in mind the known magnetic moments of Li^{1+} (0 μ_B), Co^{2+} (3 μ_B), Dy^{3+} (10.5 μ_B) and Fe^{3+} (5 μ_B) the variation in saturation magnetization with substituent concentration, x, can be explained. The saturation magnetization decreases with increasing Co^{2+} substitution. The introduction of Co^{2+} ions in place of Fe^{3+} ions into the preferred octahedral B-sites and reduction in the percentage content of nonmagnetic lithium ions at constant percent of dysprosium ions at octahedral sites, dilute both the A and B sublattices simultaneously. The net magnetization, being the difference between A and B sublattice magnetizations, is observed to decrease due to the smaller dilution of Fe^{3+} ions at B-site. The incorporation of Co^{2+} ions into the A-sublattice and B-sublattice leads to larger decrease in magnetic moment of A-sublattice as compared to that of B-sublattice so that the total magnetic moment decreases. The remanent ratio $R = M_r/M_s$ is a characteristic parameter of the material. High remanent ratio is desirable for magnetic recording and memory devices. It is an indication of the ease with which the direction of magnetization reorients to nearest easy axis magnetization direction after the magnetic field is removed. Lower value of the remanent ratio is an indication of isotropic nature of material. It is observed that the values of R in the present case are in the range of 0.31–0.64 and shows increasing trend with Co^{2+} substitution. It is clearly observed from Figs. 6 and 7 that the coercivity increases as Co^{2+} substitution increases. The H_c is basically increased from 103 Oe and attains a large value of 812 Oe with increasing Co^{2+} ions. This is due to the fact that H_c is enhanced by enlarging the magnetocrystalline anisotropy. The behavior of coercivity is similar to that of porosity. Porosity affects the magnetization process because pores work as a generator of demagnetizing field. As the porosity increases, a higher field is needed to push the domain wall, increasing H_c. The saturation magnetization is related to H_c through Brown's relation [41]

$$H_c = \frac{2K_1}{\mu_0 M_s} \tag{8}$$

According to this relation H_c is inversely proportional to M_s, which is consistent with our experimental results. The magnetocrystalline anisotropy constant (K_1) of cobalt ferrite is very large [42] and Li ferrite is small [43]. The total anisotropy equals to the difference between their anisotropies. Therefore, anisotropy increased with the replacement of Li ion by Co ion, which implies an increase in H_c.

The observed magnetic moment ($n_B$obs.) per formula unit in the Bohr magneton (μ_B) was calculated experimentally using a relation [44]

$$n_B\text{obs.} = \frac{Molecular\ weight \times M_s}{5585 \times \rho_{th}} \tag{9}$$

where ρ_{th} is the bulk density of the sintered sample. The calculated magnetic moment ($n_B$cal.) per formula unit in μ_B is expressed as $n_B\text{cal.} = M_{B(x)} - M_{A(x)}$ where M_B and M_A are the B and A sublattice magnetic moments in μ_B. Values of the calculated magnetic moment ($n_B$cal.) were calculated by considering the magnetic moments of constituent ions. The variation of calculated and observed magneton number is presented in Fig. 8. It is observed that the experimental values are in good agreement with the calculated results. The magnetic moment supposed to decrease as the Co^{2+} content increases; this can be explained on the basis of magnetic moment of the constituent ions. When x amount of cobalt ion is added, the percent Fe^{3+} ions are comparatively decreased from B-site by an larger amount as compared to A-site. Hence the addition of cobalt ions

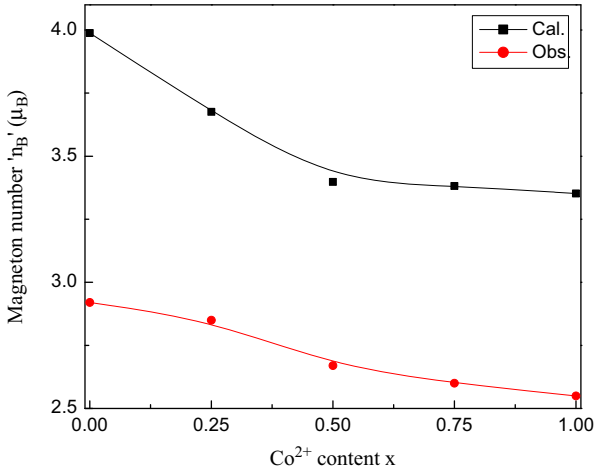

Fig. 8. Variation of observed (obs.) and calculated (cal.) magneton number with Co^{2+} content x.

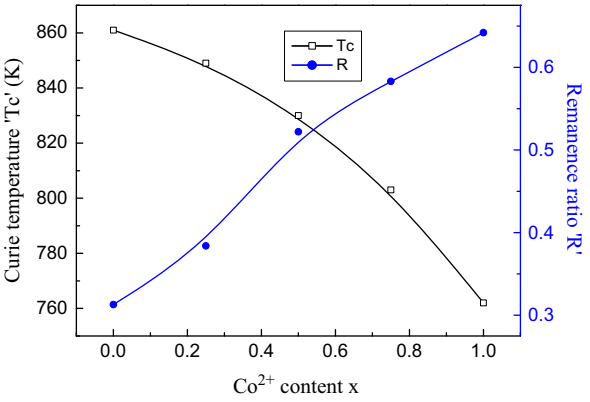

Fig. 9. Variation of Curie temperature (T_c) and remanence ratio (R) with Co^{2+} content x.

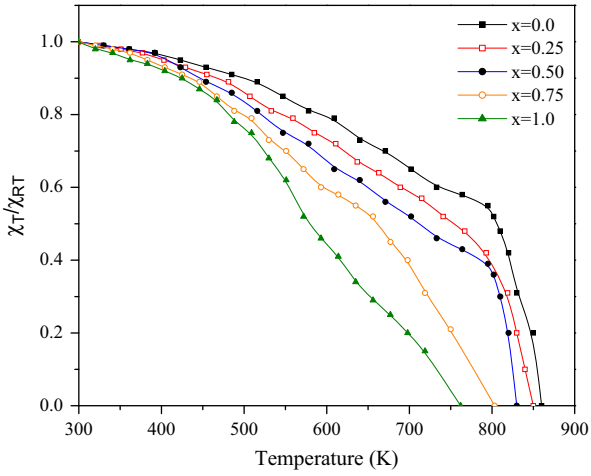

Fig. 10. Plots of χ_T/χ_{RT} for $Li_{0.5-0.5x}Co_xFe_{2.4-0.5x}Dy_{0.1}O_4$.

decreases the difference between A- and B-sublattices magnetic moment.

Method of preparation, chemical composition, microstructure and grain size play a crucial role in deciding the magnetic susceptibility. The thermal variation of ac susceptibility of all polycrystalline samples was obtained using a double coil setup [45]. The variation of ac susceptibility as a function of temperature and composition x is studied. Thermal variation of ac susceptibility of all the samples is shown in Fig. 10. The plots of χ_T/χ_{RT} are used to determine the Curie temperature. The variation in Curie temperature with Co^{2+} content x is as shown in Fig. 9. The Curie temperature has been observed to decrease with the increase in the Co^{2+} substituent ions. The decrease in Curie temperature is almost linear.

4. Conclusions

The experimental results obtained on $Li_{0.5-0.5x}Co_xFe_{2.4-0.5x}Dy_{0.1}O_4$ spinel ferrite system lead to draw the following conclusions.

The X-ray diffraction patterns of $Li_{0.5-0.5x}Co_xFe_{2.4-0.5x}Dy_{0.1}O_4$ show secondary phases which may be due to the presence of rare earth (Dy^{3+}) ion. The cation distribution data suggest that Dy^{3+} distributed over both the sites and showing preference toward octahedral [B] site. The infrared spectra revealed the presence of two main absorption bands showing the characteristic features of spinel ferrites. The SEM micrographs of all the samples exhibit exaggerated grain growth with a dense structure. The saturation magnetization and Curie temperature decrease with increase in Co^{2+} content due to the weakening in A–B interactions. Coercivity increases due to enhancement in magnetocrystalline anisotropy with Co^{2+} substitution.

References

[1] Alex Goldman, Modern Ferrite Technology, 2nd ed., Springer, New York, 2006.
[2] Sagar E. Shirsath, R.H. Kadam, Anil S. Gaikwad, Ali Ghasemi, Akimitsu Morisako, Effect of sintering temperature and the particle size on the structural and magnetic properties of nanocrystalline $Li_{0.5}Fe_{2.5}O_4$, Journal of Magnetism and Magnetic Materials 323 (2011) 3104–3108.
[3] R.H. Kadam, A.R. Biradar, M.L. Mane, Sagar E. Shirsath, Sol–gel auto-combustion synthesis of $Li_{3x}MnFe_{2-x}O_4$ and their characterizations, Journal of Applied Physics 112 (2012) 043902.
[4] Z.C. Xu, Magnetic anisotropy and Mössbauer spectra in disordered lithium–zinc ferrites, Journal of Applied Physics 93 (2003) 4746–4749.
[5] S.H. Gee, Y.K. Hong, M.H. Park, D.W. Erickson, P.J. Lamb, Synthesis of nanosized $(Li_{0.5x}Fe_{0.5x}Zn_{1-x})Fe_2O_4$ particles and magnetic properties, Journal of Applied Physics 91 (2002) 7586–7588.
[6] Sagar E. Shirsath, Synthesis condition reflected structural and magnetic properties of $Li_{0.5}Cr_{0.5}Fe_2O_4$ nanoparticles, in: Beate Acklin, Edon Lautens (Eds.), Magnetic Nanoparticles: Properties, Synthesis and Applications, Nova Publishers, New York, 2012, pp. 205–226.
[7] E. Wolska, P. Piszora, W. Nowicki, J. Darul, Vibrational spectra of lithium ferrites: infrared spectroscopic studies of Mn-substituted $LiFe_5O_8$, International Journal of Inorganic Materials 3 (2001) 503–507.
[8] G.M. Argentina, P.D. Baba, Microwave lithium ferrites: an overview, IEEE Transactions on Microwave Theory and Techniques 22 (1974) 652–658.
[9] J.M. Song, J.G. Koh, Studies of polycrystalline cobalt-substituted lithium ferrites, IEEE Transactions on Magnetics 32 (1996) 411–415.
[10] Mamata Maisnam, Sumitra Phanjoubam, H.N.K. Sarma, Chandra Prakash, L. Radhapiyari Devi, O.P. Thakur, Magnetic properties of vanadium-substituted lithium zinc titanium ferrite, Materials Letters 58 (2004) 2412–2414.
[11] P. Kishan, in: V.R.K. Murthy (Ed.), Microwave Materials, Narosa Publishing House, New Delhi, India, 1993.
[12] Xiwei Qi, Ji Zhou, Zhenxing Yue, Zhilun Gui, Longtu Li, Permeability and microstructure of manganese modified lithium ferrite prepared by sol–gel auto-combustion method, Materials Science and Engineering B 99 (2003) 278–281.
[13] L.A. de Picciotto, M.M. Thackeray, Lithium insertion into the spinel $LiFe_5O_8$, Materials Research Bulletin 21 (1986) 583–592.
[14] S.A. Mazen, A. Elfalaky, A.Z. Mohamed, H.A. Hashem, Effect of Ti^{4+} substitution in copper ferrite: an analogous study, Materials Chemistry and Physics 44 (1996) 293–297.
[15] Vivek Verma, S.P. Gairola, Mohan C. Mathpal, S. Annapoorni, R.K. Kotnala, Magnetic and electrical properties of manganese and

cadmium co-substituted lithium ferrites, Journal of Alloys and Compounds 481 (2009) 872–876.
[16] J.G. Booth, G. Srinivasan, C.E. Patton, C.M. Srivastava, Spin wave stiffness parameters in lithium–zinc ferrites, Solid State Communications 64 (1987) 287–289.
[17] S.S. Bellad, S.C. Watawe, B.K. Chougule, Some ac electrical properties of Li–Mg ferrites, Materials Research Bulletin 34 (1999) 1099–1106.
[18] D.R. Mane, Swati Patil, D.D. Birajdar, A.B. Kadam, Sagar E. Shirsath, R.H. Kadam, Sol–gel synthesis of Cr^{3+} substituted $Li_{0.5}Fe_{2.5}O_4$: cation distribution, structural and magnetic properties, Materials Chemistry and Physics 126 (2011) 755–760.
[19] N. Rezlescu, E. Rezlescu, P.D. Popa, L. Rezlescu, Effects of rare-earth oxides on physical properties of Li–Zn ferrite, Journal of Alloys and Compounds 275–277 (1998) 657–659.
[20] N. Rezlescu, E. Rezlescu, The influence of Fe substitutions by R ions in a Ni–Zn ferrite, Solid State Communications 88 (1993) 139–141.
[21] Sagar E. Shirsath, R.H. Kadam, S.M. Patange, M.L. Mane, Ali Ghasemi, Akimitsu Morisako, Enhanced magnetic properties of Dy^{3+} substituted Ni–Cu–Zn ferrite nanoparticles, Applied Physics Letters 100 (2012) 042407.
[22] Wang Jing, Zhang Hong, Bai Shuxin, Chen Ke, Zhang Changrui, Microwave absorbing properties of rare-earth elements substituted W-type barium ferrite, Journal of Magnetism and Magnetic Materials 312 (2007) 310–313.
[23] L.Ben Tahar, M. Artus, S. Ammar, L.S. Smiri, F. Herbst, M.-J. Vaulay, V. Richard, J.-M. Greneche, F. Villain, F. Fievet, Magnetic properties of $CoFe_{1.9}RE_{0.1}O_4$ nanoparticles (RE = La, Ce, Nd, Sm, Eu, Gd, Tb, Ho) prepared in polyol, Journal of Magnetism and Magnetic Materials 320 (2008) 3242–3250.
[24] M.A. Ahmed, Samiha T. Bishay, Conductivity improvement of Li–Co–Yb ferrite, Journal of Physics D: Applied Physics 34 (2001) 1339–1345.
[25] M.A. Ahmed, Samiha T. Bishay, The role of Dy^{3+} ions and sintering temperature on the magnetic characterization of LiCo-ferrite, Journal of Magnetism and Magnetic Materials 279 (2004) 178–183.
[26] A. Vasiliu, Gh. Maxim, M.L. Craus, E. Luca, Some magnetic properties and the phase equilibrium of the compounds in the $Ca_xNi_{1-x}Fe_2O_4$ system, Physica Status Solidi A 13 (1972) 371–376.
[27] K.Kamala Bharathi, K. Balamurugan, P.N. Santhosh, M. Pattabiraman, G. Markandeyulu, Magnetocapacitance in Dy-doped Ni ferrite, Physical Review B 77 (2008) 172401–172404.
[28] Sagar E. Shirsath, B.G. Toksha, K.M. Jadhav, Structural and magnetic properties of In^{3+} substituted $NiFe_2O_4$, Materials Chemistry and Physics 117 (2009) 163–168.
[29] B.S. Chauhan, R. Kumar, K.M. Jadhav, M. Singh, Magnetic study of substituted Mg–Mn ferrites synthesized by citrate precursor method, Journal of Magnetism and Magnetic Materials 283 (2004) 71–81.
[30] L. Weil, E.F. Bertaut, L. Bochirol, Propriétés magnétiques et structure de la phase quadratique du ferrite de cuivre, Journal de Physique et le Radium 11 (1950) 208–212.
[31] P. Porta, F.S. Stone, R.G. Turner, The distribution of nickel ions among octahedral and tetrahedral sites in $NiAl_2O_4$–$MgAl_2O_4$ solid solutions, Journal of Solid State Chemistry 11 (1974) 135–147.
[32] E. Wolska, E. Riedel, W. Wolski, The evidence of $Cd_x^{2+}Fe_{1-x}^{3+}[Ni_{1-x}^{2+}Fe_{1+x}^{3+}]O_4$ cation distribution based on X-ray and Mössbauer data, Physica Status Solidi A 132 (1992) K51–K56.
[33] S.M. Patange, Sagar E. Shirsath, B.G. Toksha, S.S. Jadhav, S.J. Shukla, K.M. Jadhav, Cation distribution by Rietveld, spectral and magnetic studies of chromium-substituted nickel ferrites, Applied Physics A: Materials Science and Processing 95 (2009) 429–434.
[34] B.D. Cullity, Elements of X-ray Diffraction, Addison-Wesley Publishing Company Inc., Reading, Massachusetts, USA, 1956, pp. 474–476.
[35] J. Smit, H.P.J. Wijn, Ferrites: Physical Properties of Ferrimagnetic Oxides in Relation to Their Technical Applications, Wiley, New York, 1959.
[36] A.A. Yousef, M.E. El-Zain, S.A. Mazen, H.H. Sutherland, M.A. Abdallab, S.G. Mansour, A Mossbauer and X-ray diffraction investigation of Li–Ti ferrites, Journal of Physics Condensed Matter 6 (1994) 5717.
[37] R. Valenzuela, Magnetic Ceramics, Cambridge University Press, 1994.
[38] K.J. Standley, in: Oxide Magnetic Materials, Clarendon Press, Oxford, 1972.
[39] Brett Ammundsen, Gary R. Burns, M.Saiful Islam, Hirofumi Kanoh, Jacques Rozière, Lattice dynamics and vibrational spectra of lithium manganese oxides: a computer simulation and spectroscopic study, Journal of Physical Chemistry B 103 (1999) 5175–5180.
[40] R.D. Waldron, Infrared spectra of ferrites, Physical Review 99 (1955) 1727–1735.
[41] J.M.D. Coey, Rare Earth Permanent Magnetism, New York, John Wiley and Sons, 1996.
[42] D.R. Mane, D.D. Birajdar, Swati Patil, Sagar E. Shirsath, R.H. Kadam, Redistribution of cations and enhancement in magnetic properties of sol–gel synthesized $Cu_{0.7-x}Co_xZn_{0.3}Fe_2O_4$ ($0 \le x \le 0.5$), Journal of Sol–Gel Science and Technology 58 (2011) 70–79.
[43] S.S. Bellad, S.C. Watwe, A.M. Shaikh, B.K. Chougule, Cadmium substituted high permeability lithium ferrite, Bulletin of Materials Science 23 (2000) 83–85.
[44] Misbah Ul-Islam, T. Abbas, M.U. Rana, Magnetic properties of Cd-substituted copper ferrites, International Journal of Modern Physics B 20 (2006) 725–735.
[45] S.S. Jadhav, Sagar E. Shirsath, B.G. Toksha, S.J. Shukla, K.M. Jadhav, Effect of cation proportion on the structural and magnetic properties of Ni–Zn ferrites nano-size particles prepared by co-precipitation technique, Chinese Journal of Chemical Physics 21 (2008) 381–386.